JTAM (Jurnal Teori dan Aplikasi Matematika)
http://journal.ummat.ac.id/index.php/jtam
p-ISSN 2597-7512 | e-ISSN 2614-1175
Vol. 9, No. 2, April 2025, pp. 482-496

Forest Fires in Peatlands Analyzed from Various Perspectives: Spatial, Temporal, and Spatial-Temporal

Nur'ainul Miftahul Huda[1], Nurfitri Imro'ah[2], Muhammad Yahya Ayyash[2], Hesty Pratiwi[2]
[1]Mathematics Department, Universitas Tanjungpura, Indonesia
[2]Statistics Department, Universitas Tanjungpura, Indonesia
nurainul@fmipa.untan.ac.id

Article History:
Received : 31-12-2024
Revised : 27-03-2025
Accepted : 27-03-2025
Online : 26-04-2025

Keywords:
Spatial;
Dependence;
Peatland.

ABSTRACT

Peatland fires are characterized by the compaction of organic matter below the soil surface. If dry conditions occur, the organic matter can burn, making it difficult to extinguish the fire. This study aims to analyze peatland forest fires with three perspectives, namely temporal, spatial, and spatial-temporal. The data used is the confidence level data of hotspots in forest fires in Kubu Raya Regency, West Kalimantan from January 2014 to December 2023. The methodology used includes collecting fire data from satellite imagery and prepocessing the data. Furthermore, three different data analyzes were carried out, namely temporal, spatial, and spatial-temporal analysis. The results of the study obtained three perspectives, namely from the time period, handling of forest fire cases because they have an impact on the future as seen from the ARIMA model. Regarding spatiality, the distribution of hotspots spread to surrounding areas that were heavily affected by hotspots as seen from the contour map using Kriging interpolation. Finally, regarding spatiality and temporality, forest fire projections show that locations that are close together and have a history of being affected by forest fires have a strong potential for the distribution of forest fire cases as seen from the GSTAR space-time model.

https://doi.org/10.31764/jtam.v9i2.28884

———————— ◆ ————————

A. INTRODUCTION

Forest fires in peatlands are a significant issue that harms ecosystems, human health, and climate change (Li et al., 2023). Peatlands are also highly prone to fire. Not only do these fires inflict damage to the area's biodiversity, but they also emit significant quantities of carbon dioxide into the atmosphere, which contributes to the planet's warming (Harenda et al., 2018). There is a correlation between peatland fires and an increase in greenhouse gas emissions and an impact on air quality (Alig, 2011). Therefore, it is essential to implement sustainable land management to prevent fires and maintain the ecosystem's equilibrium.

The forest fires in West Kalimantan continue to pose a significant risk to the environment and humanity. These fires have a wide range of effects on ecosystems, population health, and the economy (Gajendiran et al., 2024). In addition to destroying natural habitats and posing a threat to biodiversity, forest fires are also responsible for releasing extremely high levels of carbon emissions into the atmosphere, contributing to global warming (Nunes, 2023). Fires that occur due to land conversion for oil palm plantations in Kalimantan cause considerable greenhouse gas emissions, affecting the air quality at both the local and regional levels (Nobre et al., 2016).

Furthermore, underlined that the haze produced by forest fires causes significant health concerns, such as respiratory illnesses, which can potentially increase medical care costs (Eusemann et al., 2013). It is becoming increasingly urgent to establish efficient forest fire prevention and management measures because the frequency of fires is growing because of climate change and the management of land that is not sustainable (Bargali et al., 2024). The progression of the number of fire hotspots in West Kalimantan over the past ten years is depicted in a bar chart that can be found in Figure 1.

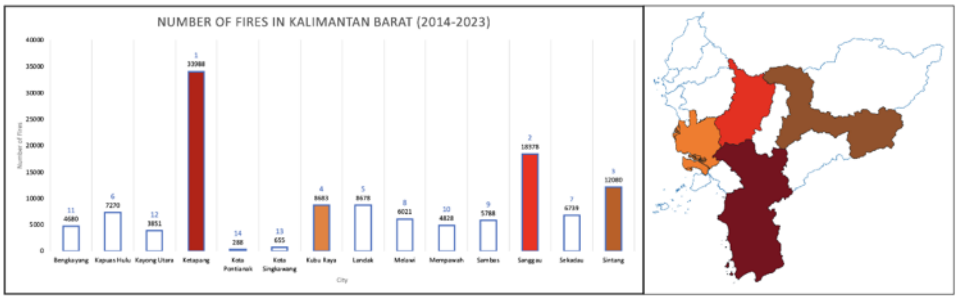

Figure 1. The Number of Forest Fires for Last Decade in Kalimantan Barat

Forest fires in West Kalimantan frequently result in peatland combustion, leading to significant environmental harm. Peatlands, crucial carbon reservoirs, become highly susceptible when incinerated, as the combustion process generates substantial carbon dioxide emissions into the atmosphere, exacerbating climate change(Hein et al., 2022). Another research demonstrated that peatland fires obliterate plants, degrade soil quality, and alter ecosystem services (Dupras et al., 2016; Page et al., 2011). Subsequently, another research emphasized that peatland fires are frequently instigated by anthropogenic activities, such as land conversion for plantations, exacerbating the issue (Dupras et al., 2016). Figure 2 shows the burned land mapping for each district/city in West Kalimantan. Kubu Raya Regency has the most land burned in the last eight years. Therefore, the object of this research is Kubu Raya Regency.

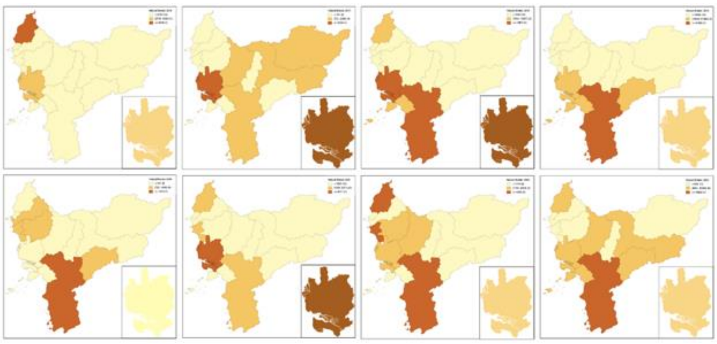

Figure 2. Burned land (2016-2023) for each district/city with three classifications: low, medium, and high burning. The darker the color, the wider the area of land that is burned

Forest fire incidents in Kubu Raya Regency can be examined through a time series methodology to identify fire patterns and trends over a specific duration. This research can identify times of elevated fire frequency by gathering historical data on fire incidences, the extent of area burned, and climatic parameters such as soil moisture and temperature. Time series models can yield significant insights into the effects of climate change and anthropogenic activities, such as land conversion for plantations, which frequently exacerbate fires (Kaur et al., 2023). Consequently, time series analysis serves to comprehend historical fire incidences and formulate more proactive and data-informed actions for the future. The incidence of forest fires in Kubu Raya Regency can be examined through spatial analysis to comprehend these occurrences' geographical distribution and patterns. By applying geospatial mapping and analysis technology, such as GIS, researchers can identify regions most susceptible to fires and the reasons for these occurrences (Parajuli et al., 2020). These factors include land use, vegetation types, and the proximity of human settlements. Geographical analysis can elucidate the correlation between forest fires and plantation land conversion, together with the impact of meteorological circumstances (Soltani & Askari, 2017).

Furthermore, fires frequently transpire in regions characterized by low soil moisture and elevated temperatures, enabling spatial analysis to forecast the probability of future fires (Suhardono et al., 2024). Spatial and temporal monitoring of forest fires might demonstrate a rising trend of fires associated with unsustainable land management practices, particularly land conversion for oil palm plantations (Gui et al., 2023). Furthermore, a spatial-temporal analysis revealed that fires are more prevalent during specific months that align with the dry season and in regions that are readily accessible for human activity (Wang et al., 2016). This study examines forest fire incidents through time series, spatial, and spatial-temporal analyses.

The significant contribution of this article is the use of three different perspectives together in analyzing a problem, namely forest fires in this context. The perspective used is spatial analysis, temporal analysis, and spatial-temporal analysis. To facilitate understanding of the results of this work, we provide an outline of this article. The background has been explained in the first section, and then the three perspectives (spatial, temporal, and spatial-temporal) are explained in general in the second section. Section 2 is also equipped with a modelling flowchart for each analysis. More details regarding the application of the three perspectives to forest fire data are explained in the third section. The results are given in the fourth section of the discussion. Finally, the conclusion of the whole thing discussed in this article is placed in the fifth section.

B. METHOD

1. Spatial

Conducting a spatial autocorrelation test between sample location points is the initial stage in the process of modelling spatial data. Moran's I is one of the most well-known indices for determining the level of spatial correlation. The values of Moran might run anywhere from -1 to 1 (Huda et al., 2023). The Moran's I statistic is given as:

$$I = \frac{N\sum_{i=1}^{n}\sum_{j=1}^{n} w_{ij}(y_i-\bar{y})(y_j-\bar{y})}{W\sum_{i=1}^{N}(y_i-\bar{y})^2} \tag{1}$$

where N is the number of known points used, y_i is interpolated (arbitrary) point, $\bar{y}$ is the mean of y, w_{ij} are the weight matrix elements, and W is the sum of all w_{ij}.

a. Kriging
   The Kriging method is an assessment technique that can be utilized to make decisions regarding scenarios involving natural phenomena (Erten et al., 2022). Simple Kriging, Ordinary Kriging, and Universal Kriging methods are suitable for tackling this issue (Fischer & Proppe, 2023; Khan et al., 2023; Ligas, 2022). Kriging is typically employed to estimate an interpolated value derived from known data points.
b. Ordinary Kriging
   Ordinary Kriging is a technique that assumes that the population's mean is unknown and always has the same value (Sukkuea & Heednacram, 2022). Ordinary Kriging presumes that the population's mean is unknown and consistently holds a value. In ordinary Kriging, spatial prediction is accomplished using assumptions (Kumar et al., 2023).

$$\hat{Z}(u_0) = \sum_{i=1}^{n} w_i Z(u_i) \tag{2}$$

   where $\sum_{i=1}^{n} w_i = 1$. One of the principal goals of the Kriging technique is to establish a best, linear, and unbiased estimate (BLUE) (M. Li et al., 2021). Figure 3.a. shows the modeling flow for spatial analysis with the input data used being spatial data at forest fire coordinate points in Kubu Raya Regency.

2. Temporal

When applied to the problem of forest fires, the ARIMA model has been utilized to forecast fire occurrences by utilizing historical data. For instance, ARIMA models could be utilized to accurately forecast forest fires in Indonesia, hence assisting stakeholders in developing more efficient measures for mitigating the effects of these fires (Glenk et al., 2017). When conducting this analysis, ARIMA was utilized to examine the emission patterns over time. ARIMA is a model combining these three components to capture stationary time series data patterns. ARIMA is one of the most effective techniques for time series analysis (Box & Jankins, 1976). This is because it can handle a variety of patterns, including seasonality and trends. Let Y_t follows the ARIMA(p, d, q) model (Sharma et al., 2024),

$$\phi(B)Y_t = \theta(B)e_t$$

since $\phi(B) = 1 - \phi_1 B - \cdots - \phi_p B^p$ and $\theta(B) = 1 - \theta_1 B - \cdots - \theta_q B^q$, then

$$Y_t = \phi_1 Y_{t-1} + \cdots + \phi_p Y_{t-p} + e_t - \theta_1 e_{t-1} - \cdots - \theta_q e_{t-q} \tag{3}$$

where $\phi_1, \dots, \phi_p$ are the parameters of Autoregressive, $\theta_1, \dots, \theta_q$ are the parameters of Moving Average. Let Y_t follows the ARIMA(1,0,1), then Y_t can be defined as:

$$Y_t = \phi Y_{t-1} + e_t - \theta e_{t-1}$$

Most of the steps involved in ARIMA modeling are identify the order, Estimation of parameters using the Least Squares technique, and diagnostic test for residuals (Imro'ah et al., 2024). Figure 3.b. provides a more in-depth and detailed representation of the ARIMA modeling steps. The input data used is temporal data about confidence level of hotspots in Kubu Raya Regency from January 2014 to December 2023.

3. Spatial-Temporal

Applying the GSTAR model for spatial-temporal analysis has emerged as a crucial approach to comprehending the patterns and dynamics of phenomena that unfold across space and time. This model offers flexibility in capturing the local and global influences of variables that interact in space and time (Fotheringham & Rogerson, 2009). The GSTAR model has been utilized to investigate both spatial and temporal factors concurrently (Yundari et al., 2020). Let $\boldsymbol{Y}_t = \{Y_i^{(i)} | i = 1, 2, \dots, N; t = 1, 2, \dots, n\}$ be a stochastics process followed GSTAR$(p; \lambda_p)$, then $\boldsymbol{Y}_t$ can be defined as

$$\boldsymbol{Y}_t = \sum_{s=1}^{p} \left[\boldsymbol{\Phi}_{s0} + \sum_{k=1}^{\lambda_s} \boldsymbol{\Phi}_{sk} \boldsymbol{W}_k \right] \boldsymbol{Y}_{t-k} + \boldsymbol{e}_t \tag{4}$$

where $\boldsymbol{W}_k$ is weight matrix.
Let $\boldsymbol{Y}_t$ follow GSTAR(1;1), then

$$\boldsymbol{Y}_t = (\boldsymbol{\Phi}_{10} + \boldsymbol{\Phi}_{11} \boldsymbol{W}) \boldsymbol{Y}_{t-1} + \boldsymbol{e}_t \tag{5}$$

Most of the steps involved in GSTAR modeling are Identify the order (also known as the order), Estimation of parameters using the Least Squares technique, and diagnostic test for residuals. More detailed modelling stages using the GSTAR model are given in Figure 3.c. The input data used in spatial-temporal analysis is spatial-temporal data for each grid in Kabupaten Kubu Raya since January 2014 to December 2023.

4. Weight Matrix

One of the most essential tools in spatial analysis is the spatial weight matrix, which assesses the interactions between locations within a geographical context (Huda & Imro'ah, 2023). Contiguity-based weight matrices are one method that is frequently utilized as a strategy (Anselin, 2010). A spatial weight matrix can be formed using several methods, one of which is queen contiguity. This approach considers two geographic units that share boundaries or corners (Huda & Imro'ah, 2023). Let Q is the queen contiguity weight matrix. For $Q = [q_{ij}]$, then

$$q_{ij} = \begin{cases} 1, if\ i\ and\ j\ are\ sharing\ boudaries\ or\ cornesr, \\ 0, other \end{cases}$$

According to the findings of the research, it is essential to select the appropriate type of weight matrix when developing a spatial regression model (Anselin, 2010).

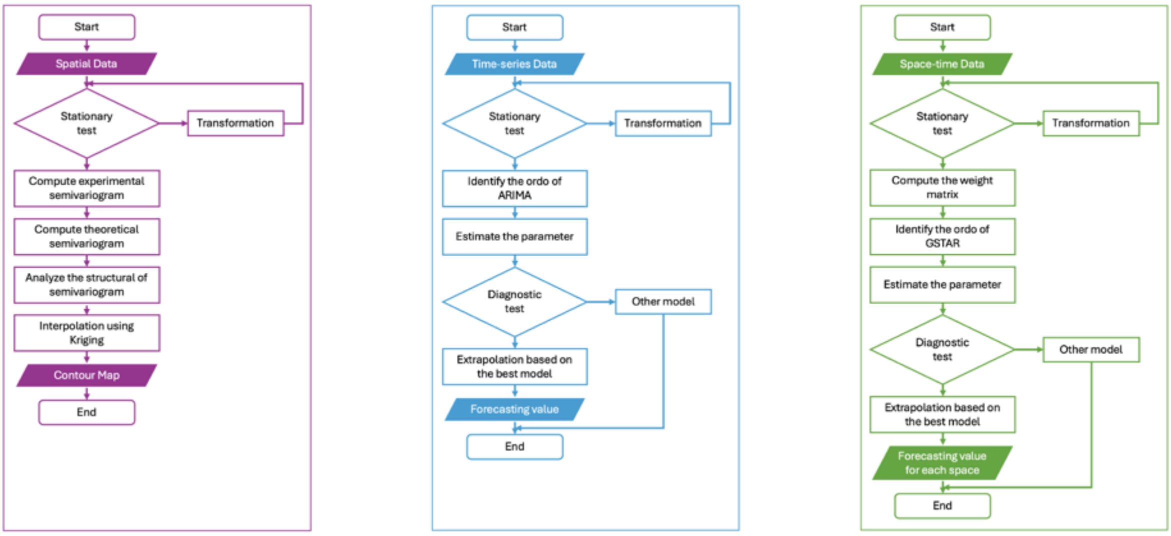

(a) Kriging (b) ARIMA (c) GSTAR

Figure 3. Flowchart of Modeling Spatial (Kriging), Temporal (ARIMA), and Spatial-Temporal (GSTAR)

C. RESULT AND DISCUSSION

In this study, secondary data were utilized, including the following: (1) Coordinate data of fire points based on satellite photography, including their longitude and latitude degrees and (2) The amount of heat that is produced by fire points daily at each point (which is, in point 1). The time span is being utilised from January 2014 to December 2023. The Kubu Raya Regency is the target location object that is being utilized. This paper presents a novel approach to determine the location, which is necessary because the spatio-temporal model assumes that there are several places within a specific period.

Prepocessing Data. This preliminary processing is designed for the purpose of conducting temporal and spatial temporal analysis. The findings of each grid are modeled using ARIMA in temporal analysis, which results in the generation of m ARIMA models (where m is the number of grid division regions). Figure 4 shows the illustration of prepocessing data. The steps involved in the preparation of data are (1) Grid. Transforming the location of Kubu Raya Regency into a square grid such that it is composed of six different regions, which are designated as A1, A2, A3, A4, A5, and A6, (2) Classification Data to Grid., and (3) Compute Average, Maximum, Number of Fires (High, Medium, Low). Figure 5 presents a time series graphic showing the outcomes of the data preprocessing performed at all six locations.

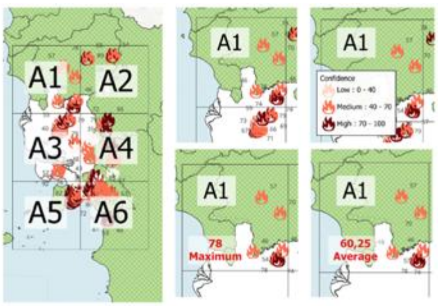

Figure 4. Prepocessing Data from the 1st - 3rd Step

The results of the data preprocessing are then computed for descriptive statistics based on two categories, namely, based on the maximum and the average value of the hotspot heat level at each location in the grid. The descriptive statistics can be found in Table 1.

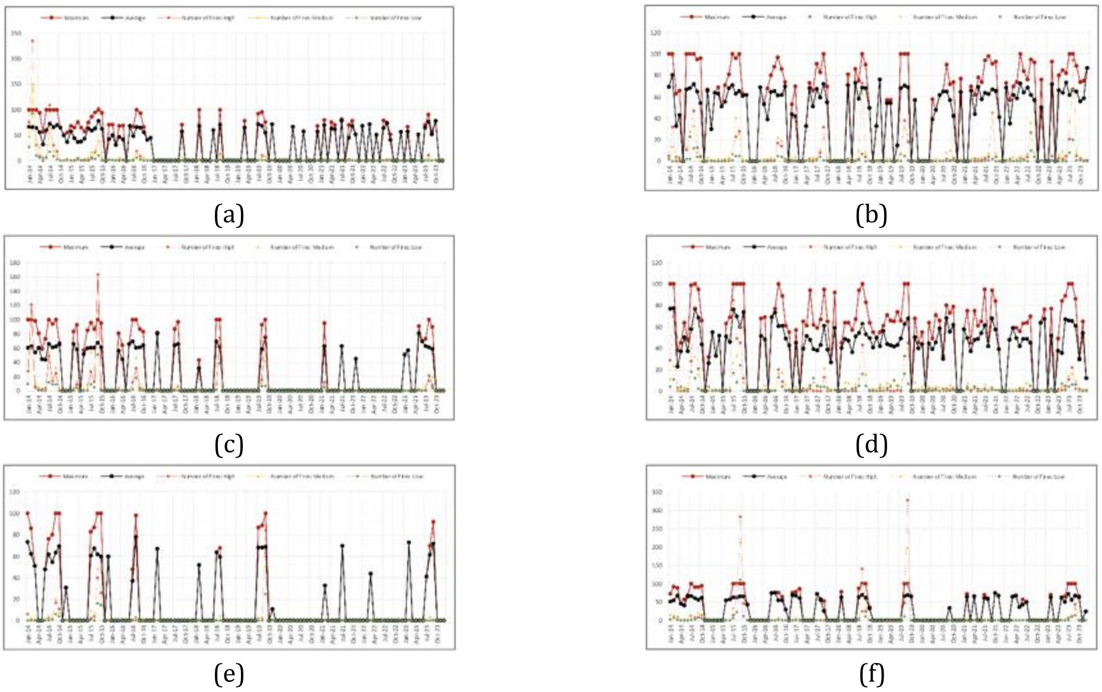

Figure 5. Time Series Data Plot for Each Grid (a) A1, (b) A2, (c) A3, (d) A4, (e) A5, and (f) A6

Tabel 1. Descriptive Statistics of Maximum and Average Value for Each Grid

Grid	A1		A2		A3		A4		A5		A6	
	Max.	**Avg.**	**Max.**	**Avg.**	**Max.**	**Avg.**	**Max.**	**Avg.**	**Max.**	**Avg.**	**Max.**	**Avg.**
Max.	100	78.21	100	87	100	81	100	77.24	100	78.20	100	76
Mean.	40.91	32.26	57.63	44.89	29.88	21.74	57.17	42.31	18.41	14.95	34.07	27.26
Var.	1544.55	936.98	1380.56	790.66	1715.21	883.84	997.28	497.73	1130.78	703.04	1536.79	927.08
Dev. Std.	39.30	30.61	37.16	28.11	41.42	29.73	31.58	22.31	33.63	26.51	39.20	30.45

1. Temporal Analysis

To begin the process of temporal modelling with ARIMA, the first thing that needs to be done is to determine the extent to which the heat level of a grid affects the time perspective. The autocorrelation value of each grid at each time lag is the basis for the tool that is used to see this (Huda et al., 2020), and it is displayed in Table 2. According to Table 2, the largest correlation is found on grid A6, which has a value of 0.550. This indicates that if a forest fire occurs today, there is a 55% chance that it will affect the forest fire the next day. Blue is used to represent the significant correlation in Table 2. Following the identification of the order of the ARIMA model by utilising the ACF and PACF plots for each grid, the subsequent step is to estimate the parameters for the model. According to Table 3, the outcomes of these stages are shown.

Tabel 2. Temporal Correlation

Grid	Time Lag									
	1	**2**	**3**	**4**	**5**	**6**	**7**	**8**	**9**	**10**
A1	.253	.357	.196	.203	.231	.267	.111	.125	.177	.051
A2	.336	.238	.057	-.172	-.252	-.266	-.256	-.127	.012	.173
A3	.529	.195	.144	.130	.173	.193	.103	.002	.004	.099
A4	.250	.087	-.112	-.189	-.172	-.192	-.166	-.138	.073	-.003
A5	.464	.195	-.030	-.108	-.027	.019	.033	-.009	-.017	.006
A6	.550	.233	.001	-.144	-.097	-.114	-.066	-.066	-.211	-.100

Afterwards, the ARIMA model order shown in Table 3 is utilised to construct an ARIMA model founded on Equation 3.

Table 3. Temporal analysis using ARIMA time series model

Grid	Order	Parameter		Diagnostic test		MAPE (%)
				Normality	Independency	
A1	(2, 1, 0)	ϕ_1	-.705	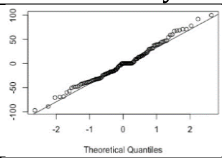	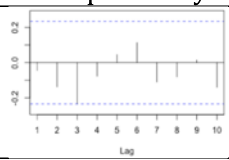	18
		ϕ_2	-.222			
A2	(0, 1, 1)	θ_1	-.569	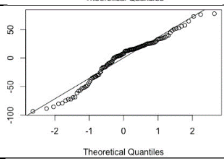	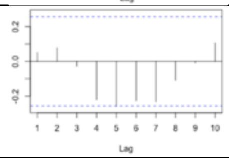	14
A3	(0, 1, 2)	θ_1	-.417	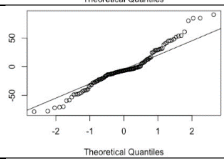	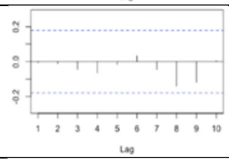	9
		θ_2	-.45817			
A4	(3, 0, 1)	ϕ_1	-.4178	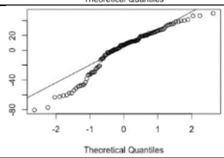	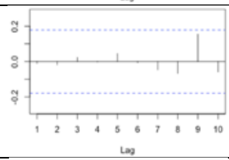	17
		ϕ_2	-.45810			
		ϕ_3	-.207			
		θ_1	-.763			
A5	(2, 1, 2)	ϕ_1	1.346	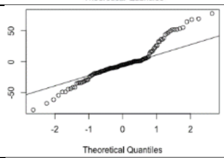	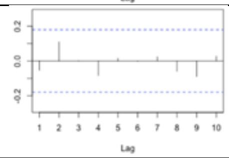	8
		ϕ_2	-.522			
		θ_1	-1.842			
		θ_2	-.871			
A6	(1, 0, 0)	ϕ_1	.550	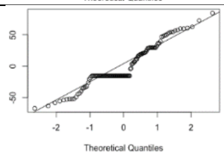	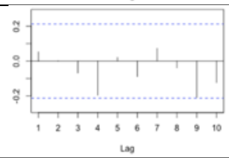	10

The parameter values presented in Table 3 are then substituted into the ARIMA model equation derived from the ARIMA model structure. The equation that represents the ARIMA model for each grid is presented below.

$$Y_t^{(1)} = -0.705Y_{(t-1)}^{(1)} - 0.222Y_{t-2}^{(1)}$$
$$Y_t^{(2)} = -0.569e_{(t-1)}^{(2)}$$
$$Y_t^{(3)} = -0.417e_{(t-1)}^{(3)} - 0.458e_{t-2}^{(3)}$$
$$Y_t^{(4)} = -0.417Y_{(t-1)}^{(4)} - 0.458Y_{t-2}^{(4)} - 0.207Y_{t-3}^{(4)} + 0.763e_{t-1}^{(4)}$$
$$Y_t^{(5)} = 1.346Y_{(t-1)}^{(1)} - 0.522Y_{t-2}^{(1)} + 1.842e_{(t-1)}^{(3)} - 0.871e_{t-2}^{(3)}$$
$$Y_t^{(6)} = 0.550Y_{t-1}^{(6)}$$

After completing the parameter estimation process, the subsequent step is to diagnostic test on the residual ARIMA model. Two tests are included in the diagnostic examination. After analysing these results, it was determined that all the developed ARIMA models could pass the diagnostic test. As a result, the model was considered to be the most effective model. Additionally, the MAPE was utilised to calculate the model's correctness (the findings are presented in Table 3). The ARIMA model on grid A5 revealed a MAPE of 6%, which indicates that the error rate produced was 6%. This was one of the six grids being produced.

2. Spatial Analysis

In the initial step of the spatial analysis process, Moran's I is utilized to perform the calculation of spatial autocorrelation. Moran's I spatial correlation outcomes for the past ten years are presented in Table 6, which can be found over here. Based on the findings, it was determined that the spatial correlation was not significant in the years 2019 and 2020 (as indicated by the red numbers), although in contrast, the spatial correlation was substantial in other years. This indicates that forest fires that occur at one point in the year have a high probability of affecting subsequent points in the year. The coordinate points and the heat levels at each point are the information used as input for spatial modelling using kriging. The data utilized for spatial modelling is presented in Table 4 and number of forest fire's points in Table 5.

Table 4. Coordinate Points of Forest Fire and Confidence Level at Each Coordinate Points

Year	MM-DD	Lat.	Long.	Conf.	...	Year	MM-DD	Lat.	Long.	Conf
2014	01-04	-0.025	109.5	23	...	2023	09-28	-0.193	109.3	42
	01-04	-0.026	109.5	74			09-28	-0.175	109.3	53
	...	...	...	...			...	...	...	...

Table 5. Number of Forest Fire's Points per Year. The bold text is the highest number of forest fire

Year	2014	2015	2016	2017	2018	2019	2020	2021	2022	2023
Total	1,116	995	221	153	**1,158**	835	42	246	68	375

The hotspot coordinates data in Table 4 is referred to as observed data. From Table 5, it is known that the total number of hotspot coordinates over the past ten years in the Kubu Raya area and its surroundings is 5,209 hotspot coordinates.

Table 6. Moran Value for Each Year. The bold text is the significant spatial correlation.

Year	2014	2015	2016	2017	2018	2019	2020	2021	2022	2023
I-Moran	0.10	0.12	0.26	0.29	**0.12**	0.00	0.04	0.12	0.12	0.16
p-value	0.00	0.00	0.00	0.00	0.00	0.37	0.12	0.00	0.00	0.00

Based on Table 6, the spatial correlation calculation results table for forest fire cases in Kubu Raya Regency and its surroundings shows that between 2014 and 2018, there was a significant clustering of hotspots, with positive I-Moran values and supporting p-values (all 0). The peak occurred in 2017 with an I-Moran value of 0.29, indicating a strong spatial relationship. The output of the spatial model analysis is a contour map of unobserved points obtained from kriging modelling based on observed points (in this case, there are 5,209 fire point coordinates). The results of the contour map using Kriging for the Kubu Raya district in 2016, 2017, 2018 and 2023 are shown in Figure 7. These years were selected based on the four highest Moran spatial correlation values in Table 6. The contour map of the kriging model results for the forest fires in Kubu Raya is a visual representation that shows the spatial distribution of fire events based on fire point data. This map connects areas with the same fire intensity through contours by using interpolation that considers location proximity and spatial variability. This reflects the potential fire risk in locations without data and shows how fire events vary depending on land type and human activity. Thus, these contour maps become essential for understanding and managing regional forest fire risk. The contour map is shown in Figure 6.

The output of contour maps using kriging for forest fire cases in Kubu Raya shows the spatial distribution of forest fire heat levels during the observed years. The data shows that longitude and latitude have consistent ranges, with longitude varying between 109.069 to 110.187 and latitude from -1.403 to 0.585. The heat level shows minimum and maximum values that vary each year; for example, 2016 recorded a minimum heat level of 0 and a maximum of 96.419, while in 2023, the heat level reached a maximum of 100, indicating a very high potential fire risk.

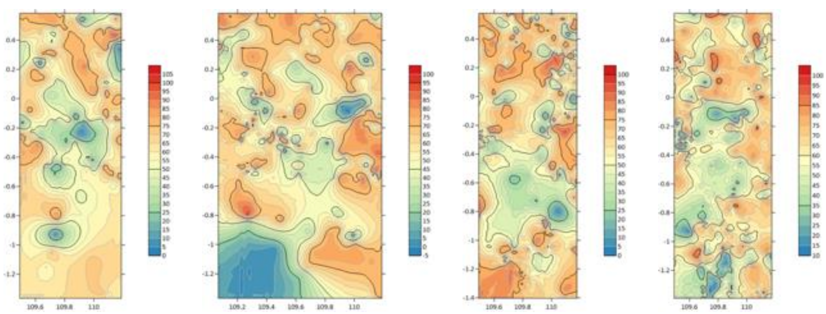

(a) (b) (c) (d)

Figure 6. Kriging Interpolation in (a) 2017, (b) 2016, (c) 2023, and (d) 2018

3. Spatial-Temporal Analysis

The environmental problem of forest fires in Kubu Raya Regency is complicated and multi-faceted. Fire events are not only driven by variables that are local to the area, but interactions between different geographical locales also influence them. Table 7 displays the spatial-temporal correlation between spatial and time lag. The correlation of 0.398 at spatial lag 0 and time lag 1 represents the relationship between forest fire cases in its own location and forest fire cases 1 time previously by 39.8%. Meanwhile, the correlation value of 0.368 at spatial lag one and time lag 1 provides information that forest fire cases in a location are related to forest fire cases in its nearest neighbouring location 1 time previously by 36.8%.

Table 7. Spatial-Temporal Correlation. The bold text is the highest spatial temporal correlation

Spatial	Time Lag									
Lag	1	2	3	4	5	6	7	8	9	10
0	**0.398**	0.228	0.059	-0.018	0.017	0.005	-0.036	-0.041	0.019	0.078
1	0.368	0.206	0.022	-0.049	-0.002	-0.023	-0.074	-0.071	-0.034	0.059

Two weight matrices are used in the case of forest fires in Kubu Raya Regency and its surroundings: the uniform weight matrix ($\boldsymbol{U}$) and the queen contiguity weight matrix ($\boldsymbol{Q}$).

$$\boldsymbol{U} = \begin{bmatrix} 0 & 0.2 & 0.2 & 0.2 & 0.2 & 0.2 \\ 0.2 & 0 & 0.2 & 0.2 & 0.2 & 0.2 \\ 0.2 & 0.2 & 0 & 0.2 & 0.2 & 0.2 \\ 0.2 & 0.2 & 0.2 & 0 & 0.2 & 0.2 \\ 0.2 & 0.2 & 0.2 & 0.2 & 0 & 0.2 \\ 0.2 & 0.2 & 0.2 & 0.2 & 0.2 & 0 \end{bmatrix}; \boldsymbol{Q} = \begin{bmatrix} 0 & 0.33 & 0.33 & 0.33 & 0 & 0 \\ 0.33 & 0 & 0.33 & 0.33 & 0 & 0 \\ 0.2 & 0.2 & 0 & 0.2 & 0.2 & 0.2 \\ 0.2 & 0.2 & 0.2 & 0 & 0.2 & 0.2 \\ 0 & 0 & 0.33 & 0.33 & 0 & 0.33 \\ 0 & 0 & 0.33 & 0.33 & 0.33 & 0 \end{bmatrix}$$

Estimating the parameters of the GSTAR(1;1) model by making use of each spatial weight ($\boldsymbol{U}$ and $\boldsymbol{Q}$) is the next phase, which can also be stated as

$$\hat{Y}_t = \begin{cases} (\hat{\Phi}_{10} + \hat{\Phi}_{11}\boldsymbol{Q})Y_{t-1} = \hat{\Phi}_Q Y_{t-1} & ,\boldsymbol{W} = \boldsymbol{Q} \\ (\hat{\Phi}_{10} + \hat{\Phi}_{11}\boldsymbol{U})Y_{t-1} = \hat{\Phi}_U Y_{t-1} & ,\boldsymbol{W} = \boldsymbol{U} \end{cases} \tag{6}$$

where $\hat{\Phi}_{10} = diag\left(\hat{\phi}_{10}^{(1)}, \dots, \hat{\phi}_{10}^{(6)}\right)$ and $\hat{\Phi}_{11} = diag\left(\hat{\phi}_{11}^{(1)}, \dots, \hat{\phi}_{11}^{(6)}\right)$

The parameters were presented in Table 8. There are three columns in Table 8: the weight matrix, the parameters of the weight matrix, and the MAPE. A comparison is then made between the two weight matrices, and the MAPE value is used to determine which model is superior. A MAPE value of 10.20% was associated with the GSTAR(1;1) model that utilised a uniform weight matrix, as indicated by the findings obtained. Based on the MAPE number, it can be deduced that the model's accuracy will result in an inaccuracy of 10.20%. In addition, the parameters that were acquired from the GSTAR(1;1) model with uniform weights (see Table 8) will be replaced into Equation 6, which will result in the model equation for each location being derived as follows:

$$\begin{aligned} Y_t^{(1)} &= 0.098Y_{t-1}^{(1)} + 0.066Y_{t-1}^{(2)} + 0.066Y_{t-1}^{(3)} + 0.066Y_{t-1}^{(4)} + 0.066Y_{t-1}^{(5)} + 0.066Y_{t-1}^{(6)} \\ Y_t^{(2)} &= 0.043Y_{t-1}^{(1)} + 0.226Y_{t-1}^{(2)} + 0.043Y_{t-1}^{(3)} + 0.043Y_{t-1}^{(4)} + 0.043Y_{t-1}^{(5)} + 0.043Y_{t-1}^{(6)} \\ Y_t^{(3)} &= 0.034Y_{t-1}^{(1)} + 0.034Y_{t-1}^{(2)} + 0.443Y_{t-1}^{(3)} + 0.034Y_{t-1}^{(4)} + 0.034Y_{t-1}^{(5)} + 0.034Y_{t-1}^{(6)} \\ Y_t^{(4)} &= 0.025Y_{t-1}^{(1)} + 0.025Y_{t-1}^{(2)} + 0.025Y_{t-1}^{(3)} + 0.184Y_{t-1}^{(4)} + 0.025Y_{t-1}^{(5)} + 0.025Y_{t-1}^{(6)} \\ Y_t^{(5)} &= 0.039Y_{t-1}^{(1)} + 0.039Y_{t-1}^{(2)} + 0.039Y_{t-1}^{(3)} + 0.039Y_{t-1}^{(4)} + 0.345Y_{t-1}^{(5)} + 0.039Y_{t-1}^{(6)} \end{aligned}$$

$$Y_t^{(5)} = 0.104Y_{t-1}^{(1)} + 0.104Y_{t-1}^{(2)} + 0.104Y_{t-1}^{(3)} + 0.104Y_{t-1}^{(4)} + 0.104Y_{t-1}^{(5)} + 0.246Y_{t-1}^{(6)}$$

Table 8. Parameter Estimation of GSTAR(1;1) Model

Weight	Parameter		MAPE
Queen Cont. (**Q**)	$\widehat{\Phi}_{10}$	$diag(0.134; 0.209; 0.443; 0.184; 0.331; 0.291)$	10.84%
	$\widehat{\Phi}_{11}$	$diag(0.261; 0.243; 0.172; 0.126; 0.205; 0.441)$	
	$\widehat{\Phi}_Q$	$\begin{bmatrix} 0 & 0.087 & 0.087 & 0.087 & 0 & 0 \\ 0.081 & 0 & 0.081 & 0.081 & 0 & 0 \\ 0.034 & 0.034 & 0 & 0.034 & 0.034 & 0.034 \\ 0.025 & 0.025 & 0.025 & 0 & 0.025 & 0.025 \\ 0 & 0 & 0.068 & 0.068 & 0 & 0.068 \\ 0 & 0 & 0.147 & 0.147 & 0.147 & 0 \end{bmatrix}$	
Uniform (**U**)	$\widehat{\Phi}_{10}$	$diag(0.098; 0.226; 0.443; 0.184; 0.346; 0.264)$	**10.20%**
	$\widehat{\Phi}_{11}$	$diag(0.331; 0.213; 0.172; 0.126; 0.192; 0.519)$	
	$\widehat{\Phi}_U$	$\begin{bmatrix} 0 & 0.066 & 0.066 & 0.066 & 0.066 & 0.066 \\ 0.043 & 0 & 0.043 & 0.043 & 0.043 & 0.043 \\ 0.034 & 0.034 & 0 & 0.034 & 0.034 & 0.034 \\ 0.025 & 0.025 & 0.025 & 0 & 0.025 & 0.025 \\ 0.038 & 0.038 & 0.038 & 0.038 & 0 & 0.038 \\ 0.104 & 0.104 & 0.104 & 0.104 & 0.104 & 0 \end{bmatrix}$	

The next step is to conduct a diagnostic test on the residuals obtained from the GSTAR (1;1) Model. The tests conducted are normality tests (using the Normal Q-Q plot) and independence (using the ACF plot) of the residual data. All locations indicate compliance with the assumptions of normality and independence of residuals. Based on the three perspectives used in analyzing peatland forest fire cases in Kubu Raya, although the three analyses provide different outputs, the conclusion of the three is that handling forest fires must be prioritized. From the temporal side, the correlation between time lags shows that almost every grid used shows a significant correlation between 1 month. Even on grid A1, within two months, forest fire cases still have a high correlation value. This finding shows that the handling of forest fire cases that occurred in Kubu Raya is still slow because, within 1 - 2 months, fire cases that have occurred still affect more than 30% of forest fire cases that occur in the following month. This is linear with the results obtained from the ARIMA model, namely on grid A4, forest fire cases that occurred this month were still influenced by 20%by forest fires that occurred in the previous three months, 45% of forest fires that occurred in the previous two months, and 41% forest fires that occurred one month earlier. Furthermore, from the spatial side, there are four years with fire cases with high spatial correlation values, namely 2016, 2017, 2018, and 2023. From these four years, several points can be seen that are the centre of forest fires. Finally, from the spatial-temporal side, the results of the analysis obtained that forest fire cases that occur in one grid have great potential to spread to adjacent grids and have great potential to increase the confidence level value based on forest fires that have occurred in previous periods. Grid location A3 shows the effect of the influence of forest fire cases that occurred in the previous month of 44.3%. At the same time, the effect of forest fire cases that occur in locations around A3 will influence 3.4%. From these three perspectives, the results show that if a forest fire occurs in one location, the handling must be carried out in less than one month, and the location with the centre of the forest fire is a priority location for handling forest fire cases.

D. CONCLUSION AND SUGGESTIONS

Peatland forest fire patterns firstly can be temporally analysed using the ARIMA model, which locates trends, cycles, and fluctuations in fire activity over time. Based on the findings of the ARIMA model analysis in forest fire instances, it was discovered that forest fire cases had been influenced around three months before the current time period. One limitation of ARIMA is that it only considers temporal patterns and does not consider geographical factors. A comprehensive understanding of the geographical distribution of forest fires in peatlands can be obtained using Kriging as a spatial interpolation approach. Using spatial data, Kriging can forecast hotspots or regions at a high risk of fire based on the locations of previously reported incidents. Based on spatial analysis, it was concluded that areas with a high confidence level have a large chance of spreading to the surrounding areas, which can be seen on the contour map. On the other hand, this approach is primarily concerned with geographical characteristics and only considers changes in time. A more detailed understanding of how peatland fire patterns develop over time and in different areas can be obtained using the GSTAR model, which incorporates time and space dimensions. The GSTAR model considers the relationship between geographical and temporal changes, enabling more accurate future fire risk projections by considering both space and time aspects concurrently.

REFERENCES

Alig, R. J. (2011). Land Use and Climate Change: A Global Perspective on Mitigation Options: Discussion. *American Journal of Agricultural Economics*, *93*(2), 356–357. https://doi.org/10.1093/ajae/aaq085

Anselin, L. (2010). Local Indicators of Spatial Association-LISA. *Geographical Analysis*, *27*(2), 93–115. https://doi.org/10.1111/j.1538-4632.1995.tb00338.x

Bargali, H., Pandey, A., Bhatt, D., Sundriyal, R. C., & Uniyal, V. P. (2024). Forest fire management, funding dynamics, and research in the burning frontier: A comprehensive review. *Trees, Forests and People*, *16*, 100526. https://doi.org/10.1016/j.tfp.2024.100526

Box, G. E. P., & Jankins, G. M. (1976). *Time Series Analysis Forecasting and Control*. Wiley.

Dupras, J., Marull, J., Parcerisas, L., Coll, F., Gonzalez, A., Girard, M., & Tello, E. (2016). The impacts of urban sprawl on ecological connectivity in the Montreal Metropolitan Region. *Environmental Science & Policy*, *58*, 61–73. https://doi.org/10.1016/j.envsci.2016.01.005

Erdogan Erten, G., Yavuz, M., & Deutsch, C. V. (2022). Combination of Machine Learning and Kriging for Spatial Estimation of Geological Attributes. *Natural Resources Research*, *31*(1), 191–213. https://doi.org/10.1007/s11053-021-10003-w

Eusemann, P., Petzold, A., Thevs, N., & Schnittler, M. (2013). Growth patterns and genetic structure of Populus euphratica Oliv. (Salicaceae) forests in NW China – Implications for conservation and management. *Forest Ecology and Management*, *297*, 27–36. https://doi.org/10.1016/j.foreco.2013.02.009

Fischer, M., & Proppe, C. (2023). Enhanced universal kriging for transformed input parameter spaces. *Probabilistic Engineering Mechanics*, *74*, 103486. https://doi.org/10.1016/j.probengmech.2023.103486

Fotheringham, A., & Rogerson, P. (2009). *The SAGE Handbook of Spatial Analysis*. SAGE Publications, Ltd. https://doi.org/10.4135/9780857020130

Gajendiran, K., Kandasamy, S., & Narayanan, M. (2024). Influences of wildfire on the forest ecosystem and climate change: A comprehensive study. *Environmental Research*, *240*, 117537. https://doi.org/10.1016/j.envres.2023.117537

Glenk, K., Shrestha, S., Topp, C. F. E., Sánchez, B., Iglesias, A., Dibari, C., & Merante, P. (2017). A farm level approach to explore farm gross margin effects of soil organic carbon management. *Agricultural Systems*, *151*, 33–46. https://doi.org/10.1016/j.agsy.2016.11.002

Gui, D., He, H., Liu, C., & Han, S. (2023). Spatio-temporal dynamic evolution of carbon emissions from land use change in Guangdong Province, China, 2000–2020. *Ecological Indicators*, *156*, 111131. https://doi.org/10.1016/j.ecolind.2023.111131

Harenda, K. M., Lamentowicz, M., Samson, M., & Chojnicki, B. H. (2018). *The Role of Peatlands and Their Carbon Storage Function in the Context of Climate Change* (pp. 169–187). https://doi.org/10.1007/978-3-319-71788-3_12

Hein, L., Spadaro, J. V., Ostro, B., Hammer, M., Sumarga, E., Salmayenti, R., Boer, R., Tata, H., Atmoko, D., & Castañeda, J.-P. (2022). The health impacts of Indonesian peatland fires. *Environmental Health*, *21*(1), 62. https://doi.org/10.1186/s12940-022-00872-w

Huda, N. M., & Imro'ah, N. (2023). Determination of the best weight matrix for the Generalized Space Time Autoregressive (GSTAR) model in the Covid-19 case on Java Island, Indonesia. *Spatial Statistics*, *54*, 100734. https://doi.org/10.1016/j.spasta.2023.100734

Huda, N. M., Imro'ah, N., & Mailanda, R. (2023). *Spatial autocorrelation using Moran's Index to map the confirmed positive of Covid-19 cases in Java*. 050006. https://doi.org/10.1063/5.0112014

Huda, N. M., Mukhaiyar, U., & Pasaribu, U. S. (2020). *Forecasting dengue fever cases using autoregressive distributed lag model with outlier factor*. 020005. https://doi.org/10.1063/5.0018450

Imro'ah, N., Huda, N. M., Utami, D. S., Umairah, T., & Arini, N. F. (2024). Control Chart for Correcting the ARIMA Time Series Model of GDP Growth Cases. *JTAM (Jurnal Teori Dan Aplikasi Matematika)*, *8*(1), 312. https://doi.org/10.31764/jtam.v8i1.19612

Kaur, J., Parmar, K. S., & Singh, S. (2023). Autoregressive models in environmental forecasting time series: a theoretical and application review. *Environmental Science and Pollution Research*, *30*(8), 19617–19641. https://doi.org/10.1007/s11356-023-25148-9

Khan, M., Almazah, M. M. A., EIlahi, A., Niaz, R., Al-Rezami, A. Y., & Zaman, B. (2023). Spatial interpolation of water quality index based on Ordinary kriging and Universal kriging. *Geomatics, Natural Hazards and Risk*, *14*(1). https://doi.org/10.1080/19475705.2023.2190853

Kumar, P., Rao, B., Burman, A., Kumar, S., & Samui, P. (2023). Spatial variation of permeability and consolidation behaviors of soil using ordinary kriging method. *Groundwater for Sustainable Development*, *20*, 100856. https://doi.org/10.1016/j.gsd.2022.100856

Leknoi, U., & Likitlersuang, S. (2020). Good practice and lesson learned in promoting vetiver as solution for slope stabilisation and erosion control in Thailand. *Land Use Policy*, *99*, 105008. https://doi.org/10.1016/j.landusepol.2020.105008

Li, L., Sali, A., Noordin, N. K., Ismail, A., & Hashim, F. (2023). Prediction of Peatlands Forest Fires in Malaysia Using Machine Learning. *Forests*, *14*(7), 1472. https://doi.org/10.3390/f14071472

Li, M., Shen, S., Barzegar, V., Sadoughi, M., Hu, C., & Laflamme, S. (2021). Kriging-based reliability analysis considering predictive uncertainty reduction. *Structural and Multidisciplinary Optimization*, *63*(6), 2721–2737. https://doi.org/10.1007/s00158-020-02831-w

Ligas, M. (2022). Comparison of kriging and least-squares collocation – Revisited. *Journal of Applied Geodesy*, *16*(3), 217–227. https://doi.org/10.1515/jag-2021-0032

Nobre, C. A., Sampaio, G., Borma, L. S., Castilla-Rubio, J. C., Silva, J. S., & Cardoso, M. (2016). Land-use and climate change risks in the Amazon and the need of a novel sustainable development paradigm. *Proceedings of the National Academy of Sciences*, *113*(39), 10759–10768. https://doi.org/10.1073/pnas.1605516113

Nunes, L. J. R. (2023). The Rising Threat of Atmospheric CO2: A Review on the Causes, Impacts, and Mitigation Strategies. *Environments*, *10*(4), 66. https://doi.org/10.3390/environments10040066

Page, S. E., Rieley, J. O., & Banks, C. J. (2011). Global and regional importance of the tropical peatland carbon pool. *Global Change Biology*, *17*(2), 798–818. https://doi.org/10.1111/j.1365-2486.2010.02279.x

Parajuli, A., Gautam, A. P., Sharma, S. P., Bhujel, K. B., Sharma, G., Thapa, P. B., Bist, B. S., & Poudel, S. (2020). Forest fire risk mapping using GIS and remote sensing in two major landscapes of Nepal. *Geomatics, Natural Hazards and Risk*, *11*(1), 2569–2586. https://doi.org/10.1080/19475705.2020.1853251

Sharma, A. K., Punj, P., Kumar, N., Das, A. K., & Kumar, A. (2024). Lifetime Prediction of a Hydraulic Pump Using ARIMA Model. *Arabian Journal for Science and Engineering*, *49*(2), 1713–1725. https://doi.org/10.1007/s13369-023-07976-6

Soltani, A., & Askari, S. (2017). Exploring spatial autocorrelation of traffic crashes based on severity. *Injury*, *48*(3), 637–647. https://doi.org/10.1016/j.injury.2017.01.032

Suhardono, S., Fitria, L., Suryawan, I. W. K., Septiariva, I. Y., Mulyana, R., Sari, M. M., Ulhasanah, N., & Prayogo, W. (2024). Human activities and forest fires in Indonesia: An analysis of the Bromo incident and implications for conservation tourism. *Trees, Forests and People*, *15*, 100509. https://doi.org/10.1016/j.tfp.2024.100509

Sukkuea, A., & Heednacram, A. (2022). Prediction on spatial elevation using improved kriging algorithms: An application in environmental management. *Expert Systems with Applications*, *207*, 117971. https://doi.org/10.1016/j.eswa.2022.117971

Wang, X., Huang, K., Yu, Y., Hu, T., & Xu, Y. (2016). An input–output structural decomposition analysis of changes in sectoral water footprint in China. *Ecological Indicators*, *69*, 26–34. https://doi.org/10.1016/j.ecolind.2016.03.029

Yundari, Y., Huda, N. M., Pasaribu, U. S., Mukhaiyar, U., & Sari, K. N. (2020). *Stationary Process in GSTAR(1;1) through Kernel Function Approach*. 020010. https://doi.org/10.1063/5.0016808